INVERSE HALFTONING BASED ON THE ANISOTROPIC *LPA-ICI* DECONVOLUTION

Alessandro Foi, Vladimir Katkovnik, Karen Egiazarian and Jaakko Astola

Signal Processing Laboratory, Tampere University of Technology, P.O. Box 553, 33101 Tampere, Finland
e-mail: firstname.lastname@tut.fi

ABSTRACT

A new inverse halftoning algorithm for restoring a continuous tone image from a given error diffusion halftone image is presented. The algorithm is based on a novel anisotropic deconvolution strategy [14, 15]. The linear model of error diffusion halftoning proposed by Kite et al. [19] is exploited. It approximates error diffusion as the sum of the convolution of the original grayscale image with a specific kernel and colored random noise. Under this model the inverse halftoning can be therefore formulated as a special deconvolution problem.

The deconvolution is performed following the *RI-RWI* (regularized inverse-regularized Wiener inverse) scheme [14] and exploiting the recently introduced anisotropic *LPA-ICI* estimator [15]. This adaptive varying scale estimator, based on the directional local polynomial approximation (*LPA*) technique and the intersection of confidence intervals (*ICI*) scale selection algorithm, allows near optimal edge adaptation. As a result, the reconstructed continuous tone image presents smooth areas faithful to the unknown original and yet preserves all the details found in the halftone. Conventional inverse-halftoning algorithms often produce estimates that are either oversmooth (loss of details) or still noisy.

Simulation experiments confirm the state-of-the-art performance of the proposed algorithm, both visually and in mean-squared-error sense.

1. INTRODUCTION

In the last two decades the color-depth of digital images, graphic cards, computer displays and digital cameras has steadily increased. The current standard for consumer devices is 8 or more bits for each color channel. In particular, for grayscale images this is equivalent to 256 or more different intensity values. Since the human eye is usually not able to distinguish between so close adjacent shades of gray, such grayscale images are often called *continuous tone* images. Coarser palettes are nowadays considered only for lossy image/video compression applications.

Despite this progress, many output and rendition devices are still unable to reproduce these continuous tone shades and can provide only a binary (black-and-white) output. Typical examples of such devices are office and industrial printers but also low-cost displays for mobile devices.

Digital halftoning is the rendition process of a continuous tone into a binary image. Although the naive approach where shades lighter or darker than a 50% gray level are thresholded, respectively, to white or black, is the simplest to implement, it is almost never used because of its visually poor result on photographic images. Taking into account the characteristics of the human visual system, which acts as low-pass filter, halftones are generated in such a way that the difference between the halftoned binary image and the original grayscale image is compacted into the high frequency end of the Fourier spectrum.

Halftoning techniques include ordered dithering or screening (dispersed-dot and clustered-dot), error diffusion, blue-noise dithering [29], and direct binary search [1]. The latter is known to provide the highest quality halftones. However the most widely used methods, because of their computational efficiency, are order dithering and error diffusion. Figure 1 illustrates the halftoning process.

Halftoned images may look good printed on paper. However, due to their high frequency characteristics they cannot be used in many situations. For example, scanning and reprinting an high-resolution halftone would result in a poor quality output (see, for example, the left column of Figure 9). Halftones, when displayed on a computer screen (which has a resolution significantly inferior to that of printer) present evident aliasing artifacts. Further processing, such as resizing or contrast enhancement, can severely degrade the image quality. Moreover, standard compression techniques are not able to process halftones efficiently. The development of applications such as high-quality digital archive of old newspapers or scientific journals can thus still be considered as challenging tasks. In all these cases it would be desirable to process, whenever available, the original grayscale image rather than the black and white halftone.

Inverse halftoning is the reconstruction process of a continuous tone image from its binary halftone, as illustrated in Figure 1. It is clear, from the above discussion, that inverse halftoning should mimick the human visual system. Thus, all inverse halftoning techniques perform some sort of low-pass filtering. A fixed-kernel low-pass filtering is simple to implement, nevertheless very seldom yields satisfactory results. In the recent years inverse halftoning has gained renewed interest and several new adaptive methods have been proposed [32]. They include thresholding in transform domain [25, 26], projection onto convex sets (POCS) [9, 2], MAP projection [31], anisotropic diffusion [20] and look-up tables (LUT) based on learning/training [23, 24, 16].

In this paper, we present a novel inverse halftoning technique combining a linear model for error diffusion [20] and the recently proposed anisotropic deconvolution scheme based on the regularized inverse-regularized Wiener inverse (*RI-RWI*) *LPA-ICI* [14, 15]. We assume that the error diffusion kernel is known. In particular, we show simulation results obtained for the Floyd-Steinberg [6] and Jarvis et al. [10] error diffusion kernels.

Just as for the traditional image deblurring problem [15], also for inverse halfotoning the anisotropic *LPA-ICI* based deconvolution yields state-of-the-art performance through a

Figure 1: An illustration of halftoning and inverse halftoning. Detail of the *Lena* image: original (left), Jarvis error diffusion halftone (center), and *LPA-ICI* estimate (*PSNR*=33.0dB) (right).

two stage, non-iterative, filtering procedure where blur and noise are simultaneously removed. The anisotropy of the proposed estimator allows to restore accurately edges and details, producing a result quite faithful to the original.

The paper is organized as follows:

- Error diffusion halftoning;
- Linear model for error diffusion;
- Deconvolution;
- Anisotropic *LPA-ICI* filtering;
- Inverse halftoning via anisotropic *LPA-ICI* deconvolution;
- Simulation results.

2. ERROR DIFFUSION

Roughly speaking, the error diffusion halftoning works by raster-scanning the continuous tone image and recursively distributing, or "diffusing", the quantization errors due to binarization on the neighboring pixels.

Let y be the original continuous tone image, x the pixel coordinate and z the halftoned image (to be generated); after setting the initial conditions [6]

$$\begin{aligned} &\tilde{y}_1 = y, \\ &x_1 = (1,1) \qquad \text{(start from top-left pixel)}, \end{aligned}$$

error diffusion is precisely defined by the following iterative procedure:

$$\begin{cases} z(x_n) = [\tilde{y}_n(x_n)]_{0,1}; \\ e_n = \tilde{y}_n(x_n) - z(x_n); \\ \tilde{y}_{n+1}(x_n + x) = \tilde{y}_n(x_n + x) + e_n h^{\mathrm{ed}}(x) \quad \forall x; \\ x_{n+1} = \mathrm{successor}(x_n); \end{cases}$$

where h^{ed} is a weight kernel, $[\cdot]_{0,1}$ is the binarization (or rounding) operation (i.e. $[\tilde{y}]_{0,1} = 1$ iff $\tilde{y} \geq \frac{1}{2}$, otherwise $[\tilde{y}]_{0,1} = 0$) and "successor" denotes the next pixel to be processed in raster-scanning.

In other words, at every step, the error diffusion algorithm

$$\begin{cases} \text{binarizes the current pixel (i.e. rounding to } \{0,1\}); \\ \text{computes the quantization error;} \\ \text{diffuses error on neighboring pixels using weights from } h^{\mathrm{ed}}; \\ \text{moves to the next pixel (in raster-scanning);} \end{cases}$$

The kernel h^{ed} is called the *error filter*. Examples of error filters are shown in Figure 2. Observe that the weights are non-zero only for those pixels that have not been already scanned. It means that the diffusion never goes backwards with respect to the scanning direction and after a pixel has been binarized its value is not modified by future iterations. The algorithm ends when the bottom-right pixel has been processed. The diffusion of the quantization error guarantees that the local averages of the halftoned z are close to the corresponding local averages of the continuous tone y.

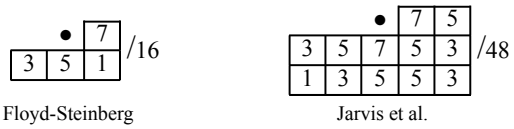

Figure 2: Error filters h^{ed} for the Floyd-Steinberg [6] (left) and Jarvis [10] error diffusions. The black dot indicates the center of the kernel.

Although the iterative nature of the procedure restricts its computational speed, on the other hand the simplicity of the iteration step, the negligible memory footprint, and the excellent rendition quality made error diffusion one of the most established halftoning techniques.

Several modifications to the above procedure (such as different pixel-scan ordering or threshold modulation) are possible [29].

3. LINEAR MODEL OF ERROR DIFFUSION

In [18] Kite et al. propose the following linear model as an approximation of error diffusion halftoning. Let Y and Z be the Fourier transforms of y and z, respectively. Then

$$Z = PY + Q\eta, \tag{1}$$

where η is white gaussian noise (with standard deviation σ),

$$P = \frac{K^{\mathrm{gain}}}{1 + \left(K^{\mathrm{gain}} - 1\right) H^{\mathrm{ed}}}, \qquad Q = \frac{1 - H^{\mathrm{ed}}}{1 + \left(K^{\mathrm{gain}} - 1\right) H^{\mathrm{ed}}},$$

H^{ed} is the frequency response of the error filter h^{ed} and K^{gain} is a gain constant. K^{gain} is found [18, 19] to be essentially independent on y and depends instead only on the used error filter: for example, $K^{\mathrm{gain}} = 2.0$ and $K^{\mathrm{gain}} = 4.5$ for the Floyd-Steinberg and Jarvis error filters respectively.

Since typical H^{ed} is a low-pass, Q is an high-pass filter (see Figure 3). This is consistent with the fact that error diffusion halftoned images differ from the continuous tone original mostly for the high frequency components of the spectrum.

The model (1) has been proved to be quite accurate [19],

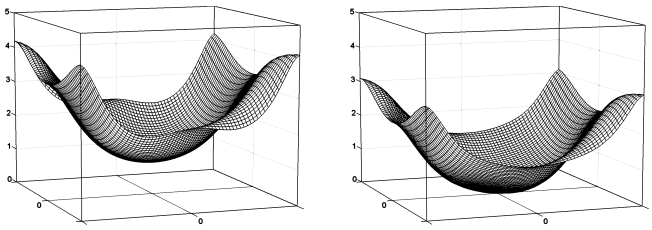

Figure 3: Absolute value of P (left) and Q (right) corresponding to the Floyd-Steinberg error filter.

and it has been already exploited in a number of algorithms (e.g. [21], [25], [26]).

3.1 Convolutional model

In the spatial domain, multiplications are replaced by convolutions and (1) becomes

$$z = p \circledast y + q \circledast \eta \tag{2}$$

where p and q are the impulse responses of P and Q respectively.

According to this model, the inverse halftoning process can be formulated as a deconvolution problem, where p is the point-spread function and the observations z are contaminated by the colored noise $q \circledast \eta$ (blue noise).

4. DECONVOLUTION

An unbiased solution of a deconvolution problem of the form (2) can be obtained in a straightforward manner by first inverting the convolution operator P and then removing the noise $P^{-1}Q\eta$. However, it is now standard to approach such inverse problems by the method of regularization, in which one applies, rather than the inversion, a regularized inverse operator [4]. A special common point of most methods starting from the frequency domain equation (1) is that some basis functions are used to approximate the object function y in the form of series with coefficients defined from the observations. These functions may be Fourier harmonics, eigenfunctions of the convolution operator in *SVD* methods or wavelets in wavelet multiresolution decompositions. There exist a lot of deconvolution techniques based on this sort of approaches.

Basically different ideas and methods arise from the pointwise nonparametric estimation approach [5]. These methods mostly do not assume any underlying global parametric model of the object and do not use the global parametric series for object approximation. It is assumed only that the object is composed from piecewise regular elements and every point of the object allows a good local approximation. The main goal of estimation is to build a pointwise approximation using the observations from a neighborhood. There is a number of proposals for nonparametric smoothing of *non-blurred* noisy images which allow for preserving the sharp edge structure as well as the edge detection and reconstruction. Actually, these methods are based on kernel smoothing with a special choice of the kernels. Spatial pointwise adaptation is now commonly considered as a crucial element of the nonparametric estimation. These adaptation methods, even for an originally linear method, are finalized in nonlinear estimators [7, 12, 22, 27]. The recently proposed *LPA-ICI deconvolution* [8, 13, 14, 15] exploits the nonparametric smoothing for a deconvolution algorithm where the regularized inversion of the convolution operation and the filtering of the noise are performed *simultaneously* in an adaptive fashion.

The anisotropic version of the *LPA-ICI* estimator [15] is a powerful tool to further improve the adaptivity of the nonparametric approach. We briefly review the basic facts of this estimator in the following section.

5. ANISOTROPIC *LPA-ICI*

5.1 Directional *LPA*

A collection of compactly supported directional *LPA* kernels $\left\{g_{h,\theta_k}\right\}_{h\in H,k=1,\ldots,K}$ is designed. Each kernel is characterized by a direction θ_k and a scale parameter h. We denote by $\hat{y}_{h,\theta_k}(x)$ the estimate obtained by filtering with the kernel g_{h,θ_k}. The *directionality* of the kernels arises from two independent facts:

- the vanishing moment conditions and the accurate polynomial reproducing properties (which characterize the *LPA*) are satisified for each kernel g_{h,θ_k} in the corresponding directions θ_k;
- the support (i.e. the windowing function) of the kernels g_{h,θ_k} is *asymmetrical* and oriented along the direction θ_k.

The elements of the collection $\left\{g_{h,\theta_k}\right\}_{h\in H,k=1,\ldots,K}$ can be grouped either *by scale* (for a fixed scale h, $\{\mathrm{supp}\, g_{h,\theta_k}\}_{k=1,\ldots,K}$ is a covering of the ball of radius h) or, as in Figures 4-5, *by direction* (for a fixed direction θ_k, $\{g_{h,\theta_k}\}_{h\in H}$ is a family of varying scale directional kernels). In our approach we follow the latter taxonomy and optimize the scale h *independently* for each direction θ_k in such a way that the noise will be suppressed as much as possible provided that the specific features of the object $y(x)$ are preserved in $\hat{y}_{h,\theta_k}(x)$.

The *ICI* rule [7] is used in order to achieve this goal in a pointwise, data-driven, manner (see e.g. [11],[12]).

5.2 *ICI* optimal scale selection algorithm

Throughout this section the direction is fixed, thus, for simplicity, we omit the index θ_k in notation.

Given an ordered set of varying scale kernel estimates $\left\{\hat{y}_{h_j}(x)\right\}_{j=1}^{J}$ with decreasing standard deviations $\sigma_{\hat{y}_{h_1}} > \cdots > \sigma_{\hat{y}_{h_J}}$ we determine a sequence of confidence intervals

$$\mathcal{D}_j = \left[\hat{y}_{h_j}(x) - \Gamma\sigma_{\hat{y}_{h_j}}, \hat{y}_{h_j}(x) + \Gamma\sigma_{\hat{y}_{h_j}}\right] \tag{3}$$

where $\Gamma > 0$ is a threshold parameter. The *ICI* rule can be stated as follows:

Consider the interesection of confidence intervals $\mathcal{I}_j = \bigcap_{i=1}^{j}\mathcal{D}_i$ *and let* j^* *be the largest of the indexes* j *for which* $\mathcal{I}_j$ *is non-empty,* $\mathcal{I}_{j^*} \neq \varnothing$ *and* $\mathcal{I}_{j^*+1} = \varnothing$. *Then the optimal scale* h^* *is defined as* $h^* = h_{j^*}$ *and the optimal scale kernel estimate is therefore* $\hat{y}_{h^*}(x)$.

Theoretical analysis produced in [7] shows that this adaptive scale gives the best possible pointwise mean-squared error. Roughly speaking, *ICI* selects the coarsest scale estimate that is statistically compatible with all finer scales. In practice this means that adaptively, for every pixel, *ICI* allows the maximum degree of smoothing, stopping before oversmoothing begins.

Optimal values of Γ in (3) can be derived from some heuristic and theoretical considerations (e.g. [11],[12],[28]).

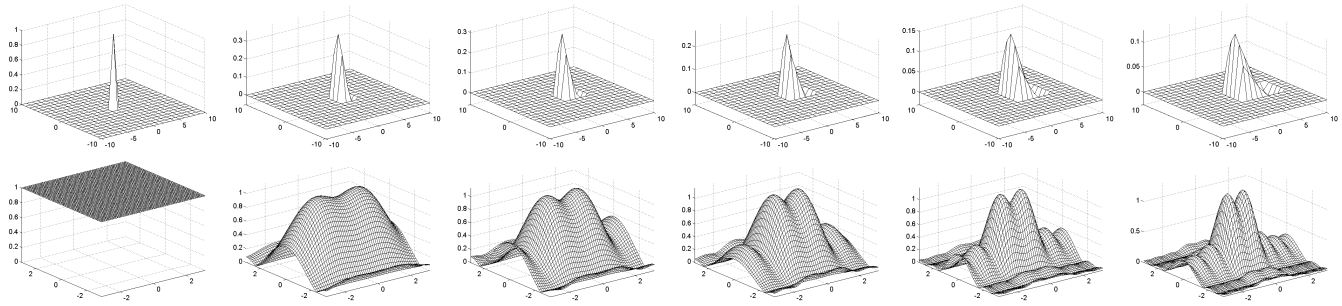

Figure 4: Varying scale *LPA* kernels (top) and the absolute value of their Fourier transforms (bottom); $m = [1,0]$, $\theta = 0$.

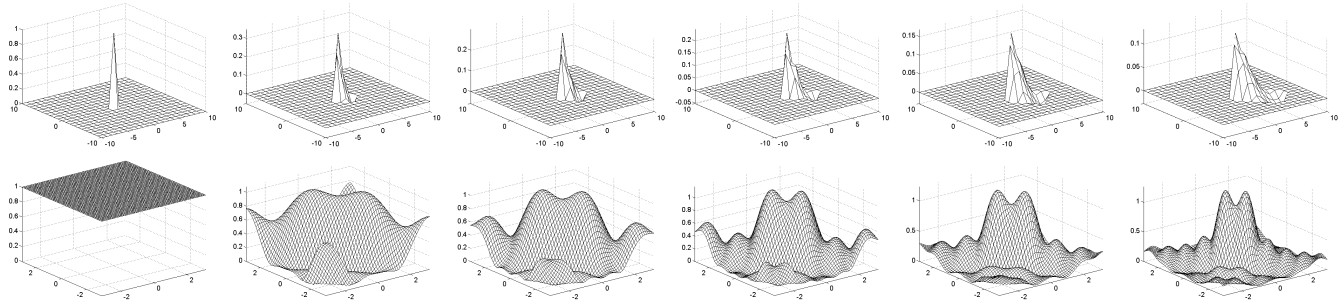

Figure 5: Varying scale *LPA* kernels (top) and the absolute value of their Fourier transforms (bottom); $m = [1,0]$, $\theta = 7\pi/4$.

However, pragmatically this sort of results is of small practical use. In this paper we prefer to treat the threshold Γ as a fixed design parameter of the inverse halftoning algorithm.

Remark: This optimal scale selection method requires the knowledge of the estimate and its variance only and is equally applicable to both introduced algorithms *RI* and *RWI*. The fast implementation of the considered algorithms is based on the calculation of the estimates $\hat{y}_{h,\theta_k}(x)$ for all x and $h \in H$ using the convolution procedure in the frequency domain and then *ICI* based selection of the best estimate for each x. This is done separately for each direction θ_k, as a result we obtain the pointwise adaptive scales $h^* = h^*(x,\theta_k)$ depending on θ_k, $k = 1,\ldots,K$.

5.3 Anisotropic estimator

Once the optimal scale estimates $\hat{y}_{h^*,\theta_k}(x)$ have been selected, the introduced anisotropic estimator has the following generic form

$$\hat{y}(x) = \sum\nolimits_k \lambda_k(x)\hat{y}_{h^*,\theta_k}(x), \quad \lambda_k(x) \geq 0,\ \sum\nolimits_k \lambda_k(x) = 1. \quad (4)$$

Formula (4) summarizes our basic intentions. We introduce the directional estimates $\hat{y}_{h,\theta_k}(x)$, optimize the scale parameter for each of the directions and then fuse these optimal directional estimates into the final one $\hat{y}(x)$ using the weights $\lambda_k(x)$.

The anisotropy of the fused estimator (4) is a direct consequence of both the asymmetrical directionality of the *LPA* kernels and the *ICI* optimal scale selection that is performed *independently* for each direction. The resulting fused estimator (4) is thus equivalent to a pointwise adaptive kernel estimator where the support of the kernel adapts to the anisotropy of the image. Figure 6 illustrates this concept showing sequentially: an ideal local estimation neighborhood U_x^*, a sectorial covering of the unit ball, and the sectorial approximation of U_x^* using the adaptive scales $h^*(x,\theta_k)$ defining the length of the corresponding sectors. The union of the asymmetrical supports of the directional kernels $g_{h^*(x,\theta_k),\theta_k}$, $\bigcup_k \operatorname{supp} g_{h^*(x,\theta_k),\theta_k}$, can be therefore considered as an approximation of the best local vicinity of x in which the estimation model fits the data [15].

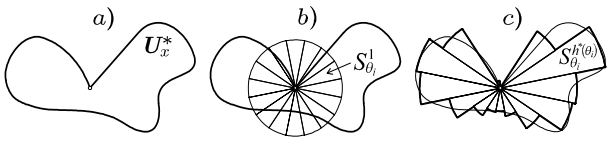

Figure 6: a) an ideal estimation neighborhood U_x^*, b) unit ball covered by sectors, c) sectorial approximation of U_x^*.

6. INVERSE HALFTONING

6.1 Adaptive deconvolution algorithm

Analogously to the previous sections, capital letters are used for the discrete Fourier transform of the corresponding functions. We denote by $\overline{P}$ the complex conjugate of P. The considered technique is based on the following regularized inversion (*RI*) and regularized Wiener inversion (*RWI*) estimates, using the directional *LPA* kernels g_{h,θ_k} :

$$\hat{Y}_{h,\theta_k}^{RI} = \frac{\overline{P} G_{h,\theta_k}}{|P|^2 + |Q|^2 \varepsilon_1^2} Z, \qquad (RI) \qquad (5)$$

$$\hat{Y}_{h,\theta_k}^{RWI} = \frac{\overline{P}|Y|^2 G_{h,\theta_k}}{|PY|^2 + \varepsilon_2^2 |Q|^2 \sigma^2} Z. \qquad (RWI) \qquad (6)$$

The adaptive procedure assumes that the estimates $\{\hat{y}_{h,\theta_k}^{RI}\}_{h \in H}$ are calculated according to (5) for a set of scales H and the *ICI* rule selects the best scales for each direction and for each pixel. In this way we obtain the

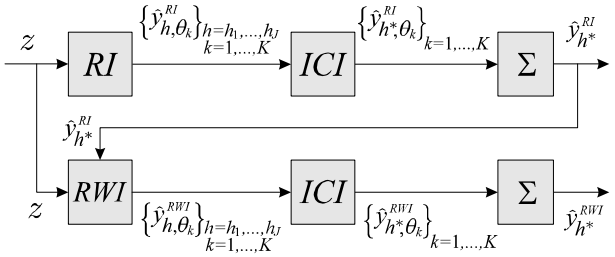

Figure 7: Directional *LPA-ICI* regularized Wiener inverse algorithm. In the first line of the flowchart the *RI* estimates are calculated for a set of scales and directions, the *ICI* is used to obtain the pointwise optimal scale directional estimates that are then fused into the $\hat{y}^{RI}_{h^*}$ estimate. In the second line the *RWI* estimates are calculated using $\hat{y}^{RI}_{h^*}$ as a reference signal in Wiener filtering, again *ICI* and fusing are performed to obtain the final $\hat{y}^{RWI}_{h^*}$ estimate.

directional varying scale adaptive estimates $\hat{y}^{RI}_{h^*(x,\theta_k),\theta_k}$, $k = 1,\dots,K$, which are fused in the final one $\hat{y}^{RI}_{h^*}$ according to (4)

$$\begin{aligned} \hat{y}^{RI}_{h^*}(x) &= \sum_k \lambda^{RI}_k(x)\hat{y}^{RI}_{h^*(x,\theta_k),\theta_k}(x), \qquad (7)\\ \lambda^{RI}_k(x) &= \sigma^{RI-2}_k(x)/\sum_i \sigma^{RI-2}_i(x), \end{aligned}$$

where σ^{RI}_k is the standard deviation of the optimal scale estimate $\hat{y}^{RI}_{h^*(x,\theta_k),\theta_k}$.

The fused $\hat{y}^{RI}_{h^*}$ serves as the reference signal in the *RWI* procedure (see Figure 7). The adaptive *RWI* algorithm is similar and gives the *ICI* adaptive varying scales estimates $\hat{y}^{RWI}_{h^*(x,\theta_k),\theta_k}$ for each direction and x. Then, the final estimate $\hat{y}^{RWI}_{h^*}$ is obtained by fusing these directional ones again similarly to (7):

$$\begin{aligned} \hat{y}^{RWI}_{h^*}(x) &= \sum_k \lambda^{RWI}_k(x)\hat{y}^{RWI}_{h^*(x,\theta_k),\theta_k}(x), \qquad (8)\\ \lambda^{RWI}_k(x) &= \sigma^{RWI-2}_k(x)/\sum_i \sigma^{RWI-2}_i(x). \end{aligned}$$

The final estimate of y of the proposed inverse halftoning algorithm is the output given by the *RWI* deconvolution scheme (6) that uses the *ICI* based *RI* estimate as a reference signal Y. Thus, we arrive to the two steps procedure shown in Figure 7.

6.2 Remarks

The *ICI* adaptive scales $h^*(\cdot,\theta_k)$ represent the distribution of image features across the direction θ_k, as shown in Figure 8 (in the figure, darker color corresponds to smaller scales). The weights λ^{RI}_k and λ^{RWI}_k in (7)-(8) are data-driven adaptive as the variances depend on the adaptive scales $h^*(x,\theta_k)$.

The variances of the estimates $\hat{y}^{RI}_{h,\theta_k}$ and $\hat{y}^{RWI}_{h,\theta_k}$ are obtained, respectively, as

$$\begin{aligned} \sigma^{RI2}_{h,\theta_k} &= \frac{\sigma^2}{n_1 n_2}\left\| \frac{\overline{P} G_{h,\theta_k} Q}{|P|^2 + |Q|^2 \varepsilon_1^2} \right\|_2^2,\\ \sigma^{RWI2}_{h,\theta_k} &= \frac{\sigma^2}{n_1 n_2}\left\| \frac{\overline{P}|Y|^2 G_{h,\theta_k} Q}{|PY|^2 + \varepsilon_2^2 |Q|^2 \sigma^2} \right\|_2^2, \end{aligned}$$

where $n_1 n_2$ is the size of the input image z, $\|\cdot\|_2$ denotes the l^2-norm, and σ^2 is the variance of the noise η in formula (1), which is assumed to be equal to 1.

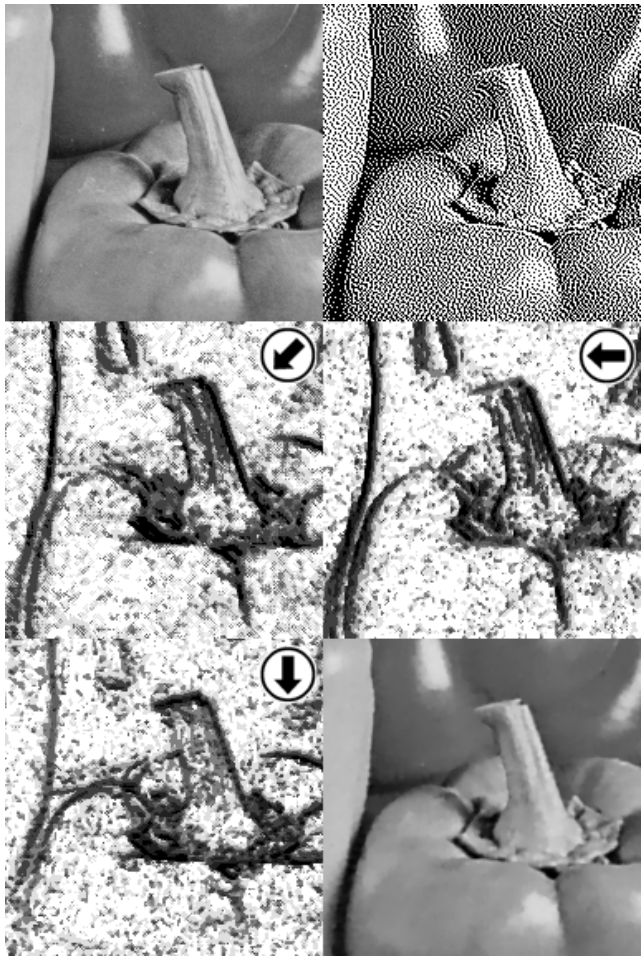

Figure 8: *Peppers* (detail): original image (top left), Jarvis error diffusion halftone (top right), optimal scales $h^*(\cdot,\pi/4)$ (center left), $h^*(\cdot,0)$ (center right), $h^*(\cdot,\pi/2)$ (bottom left), and *LPA-ICI* estimate (*PSNR*=31.6dB) (bottom right). The arrows indicate the orientation of the kernels.

6.3 Complexity

Concerning the algorithm complexity we note that the algorithm is fast as it is based on fast convolution operations. The calculation of the estimate $\hat{y}_{h_j,\theta_k}$ for a given scale h_j is a linear convolution requiring $N_{conv} \sim n \log n$ where n is the size of the signal. This procedure is repeated $J \cdot K$ times, where K is a number of directions in the estimator (4) and J is the number of the used scales h_j.

7. SIMULATION RESULTS

Directional *LPA* kernels were designed on asymmetrical windows oriented along eight directions, $\{\theta_k\}_{k=1}^8 = \{0, \pi/4, \pi/2, \dots, 7/4\pi\}$, with orders $m = [1,0]$ and $m = [0,0]$ for the *RI* and *RWI* filters respectively. A set of 6 and 9 scales was used for the *RI* and *RWI* respectively. Some of these kernels are shown in Figure 4 and 5. The first and smallest scale is always equal to 1, i.e. the kernel is the dis-

Inverse halftoning technique	*Lena*	*Peppers*
Anisotropic *LPA-ICI*	**32.4**	**31.6**
WinHD (Neelamani et al.) [26]	32.1	31.2
Wavelet-Vaguelette (Neelamani et al.) [25]	31.9	31.0
Wavelet (Xiong et al.) [30]	31.7	30.7
Gradient (Kite et al.) [20]	31.3	31.4
Kernel (Wong) [31]	32.0	30.3
LUT (Meşe and Vaidyanathan) [24]	31.0	—
LMS-MMSE (Chang et al.) [3]	31.4	31.2
POCS-SVD (Hein and Zakhor) [9]	30.4	—
POCS-Wavelet (Bozkurt and Çetin) [2]	32.2	30.9

Table 1: *PSNR* (dB) performance of the proposed algorithm and of other methods for restoration from Floyd-Steinberg error diffusion.

crete Dirac delta function.

The regularization parameters $\varepsilon_1, \varepsilon_2$, the *LPA* kernels g_{h,θ_k} and the *ICI* threshold Γ are considered as fixed design parameters of the proposed inverse halftoning algorithm. For all results and figures presented in this paper one unique set of design parameters has been used.

Although little investigation has been done in the optimization of these design parameters, our anisotropic *LPA-ICI* inverse halftoning delivers already more than satisfactory results (see Figure 9). Overall, the *PSNR* values in Table 1 show that the new developed algorithm demonstrates a good performance and outperforms some state-of-the-art techniques. Visual inspection is also in favor of the new algorithm. Figure 10 shows a fragment of the restored *Lena* image: when compared to the wavelet based inverse halftoning method [26], the proposed *LPA-ICI* procedure shows its superiority restoring finer details without introducing any visible artifacts.

Remark: Recently in [16] it has been claimed that a decision tree learning LUT algorithm can yield a *PSNR* of 34.75dB for the *Lena* image, sensibly outperforming all previous records of other authors, in particular that of the other LUT-based algorithm [24]. However, we do not include this result in table 1 as it is achieved for an usually sized 1050×1050 image. The results for the table, as well as all the figures in this paper, correspond instead to the standard 512×512 images. Nevertheless, we tested our algorithm also for the "oversized *Lena*" used in [16], obtaining a *PSNR* of 37.75dB.

REFERENCES

[1] Analoui M. and J.P. Allebach, "Model-based halftoning by direct binary search", *Proc. SPIE/IS&T Symposium on Electronic Imaging Science and Technology*, vol. 1666, pp. 96-108, 1992.

[2] Bozkurt Unal G., and A.E. Çetin, "Restoration of Error-Diffused images using Projection onto Convex Sets", *IEEE Trans. Image Processing*, December 2001.

[3] Chang P.C., C.S. Yu, and T.H. Lee,"Hybrid LMS-MMSE Inverse Halftoning Technique", *IEEE Trans. on Image Processing*, vol. 10, no. 1, pp. 95-103, Jan. 2001

[4] Engl H.W., M. Hanke and A. Neubauer, *Regularization of Inverse Problems*, Kluwer Academic Publishers, 1996.

[5] Fan J. and I. Gijbels, *Local polynomial modelling and its application*. London: Chapman and Hall, 1996.

[6] Floyd R.W., and L. Steinberg, "An Adaptive Algorithm for Spatial Greyscale", *Proc. Society for Information Display*, vol. 17, no. 2, pp. 75-77, 1976.

[7] Goldenshluger A. and A. Nemirovski, "On spatial adaptive estimation of nonparametric regression", *Math. Meth. Statistics*, vol. 6, pp. 135-170, 1997.

[8] Goldenshluger A., "On pointwise adaptive nonparametric deconvolution", *Bernoulli,* vol. 5, pp. 907-925, 1999.

[9] Hein S., and A. Zakhor, "Halftone to continuous-tone conversion of error-diffusion coded images", *IEEE Trans. on Image Processing*, vol. 4, no. 2, pp. 208-216, Feb. 1995.

[10] Jarvis J.F., C.N. Judice, and W.H. Ninke "A Survey of Techniques for the Display of Continuous Tone Pictures on Bilevel Displays", *Computer Graphics Image Processing,* 5, pp. 13-40, 1976.

[11] Katkovnik V., "A new method for varying adaptive bandwidth selection", *IEEE Trans. on Signal Proc.,* vol. 47, no. 9, pp. 2567-2571, 1999.

[12] Katkovnik V., K. Egiazarian, and J. Astola, "Adaptive window size image de-noising based on intersection of confidence intervals (ICI) rule". *J. of Math. Imaging and Vision*, vol. 16, no. 3, pp. 223-235, 2002.

[13] Katkovnik V., K. Egiazarian, and J. Astola, "A spatially adaptive nonparametric regression image deblurring", *IEEE Trans. on Image Processing* (accepted), 2004.

[14] Katkovnik V., K. Egiazarian, and J. Astola, *Adaptive varying scale methods in image processing,* Tampere International Center for Signal Processing, TICSP Series, no. 19, Tampere, TTY, Monistamo, 2003.

[15] Katkovnik V., A. Foi, K. Egiazarian and J. Astola, "Directional varying scale approximations for anisotropic signal processing", to appear in *Proceedings of EUSIPCO 2004*.

[16] Kim H.Y. and R. de Queiroz, "Inverse halftoning by decision tree learning", *Proc. IEEE Intl. Conf. on Image Processing, ICIP*, Barcelona, Spain, 2003.

[17] Kingsbury N., "Complex Wavelets for Shift Invariant Analysis and Filtering of Signals", *Applied and Computational Harmonic Analysis*, vol. 10, no. 3, pp. 234-253, May 2001.

[18] Kite T.D., B.L. Evans, T.L. Sculley, and A.C. Bovik, "Digital Image Halftoning as 2-D Delta-Sigma Modulation", *Proc. IEEE Int. Conf. on Image Processing*, 1997, Santa Barbara, CA., vol. I, pp. 799-802, 1997.

[19] Kite T.D., B.L. Evans, A.C. Bovik and T.L. Sculley, "Modeling and quality assessment of halftoning by error diffusion", *IEEE Trans. Image Proc.*, vol. 9, pp. 909-922, May 2000.

[20] Kite T.D., N. Damera-Venkata, B.L. Evans, and A.C. Bovik, "A Fast, High-Quality Inverse Halftoning Algorithm for Error Diffused Halftones", *IEEE Trans. on Image Processing*, vol. 9, no. 9, pp. 1583-1592, Sep. 2000.

[21] Kite T.D., B.L. Evans, and A.C. Bovik, "Fast rehalftoning and interpolated halftoning algorithms with flat low-frequency response", *Proceedings of International Conference on Image Processing, 1999. ICIP 99*. vol.

Figure 9: Examples of Floyd-Steinberg error diffusion *LPA-ICI* inverse halftoning: *Peppers* (*PSNR*=31.6dB), *Lena* (*PSNR*=32.4dB), and *Boats* (*PSNR*=29.5dB). The pictures in the right column are the estimates obtained by the proposed procedure from the binary halftone images (shown in the left column).

Figure 10: Visual comparison for a detail of the *Lena* image: from left to right, original and Floyd-Steinberg halftone (top), the proposed anisotropic *LPA-ICI* estimate (*PSNR*=32.4), and the "*WInHD*" estimate [26] (*PSNR*=32.1) based on deconvolution and filtering in the complex wavelet domain [17].

3, Oct. 1999.

[22] Lepski O., E. Mammen and V. Spokoiny, "Ideal spatial adaptation to inhomogeneous smoothness: an approach based on kernel estimates with variable bandwidth selection", *Annals of Statistics*, vol. 25, no. 3, pp. 929-947, 1997.

[23] Meşe M. and P.P. Vaidyanathan, "Look up table (LUT) Method for inverse halftoning", *IEEE Trans. on Image Processing*, vol. 10, no. 10, pp. 1566-1578. 2000

[24] Meşe M. and P.P. Vaidyanathan, "Tree-Structured Method for LUT Inverse Halftoning and for Image Halftoning", *IEEE Trans. on Image Processing*, vol. 11, no. 6, pp. 644-655. June 2002.

[25] Neelamani R., R. Nowak, and R. Baraniuk, "Model-based Inverse Halftoning with Wavelet Vaguelette Deconvolution", *Proc. IEEE Int. Conf. Image Processing - ICIP '00*, vol. 3, pp. 973-976, Vancouver, Canada, September 2000.

[26] Neelamani R., R. Nowak and R. Baraniuk, "WInHD: Wavelet-based Inverse Halftoning via Deconvolution", *IEEE Trans. on Image Processing*, (Submitted, October 2002).

[27] Polzehl J. and V. Spokoiny, "Image denoising: pointwise adaptive approach", *Annals of Statistics*, vol. 31, no. 1, 2003.

[28] Stanković L., "Performance Analysis of the Adaptive Algorithm for Bias-to-Variance Tradeoff", *IEEE Trans. on Signal Proc.*, vol. 52, no. 5, pp. 1228-1234, 2004.

[29] Ulichney R., *Digital Halftoning*, The MIT Press, Cambridge, Mass., 1987.

[30] Xiong Z., M.T. Orchard, and K. Ramchandran, "Inverse halftoning using wavelets", *IEEE Trans. Signal Processing*, vol. 8, pp. 1479-1482, Oct. 1999.

[31] Wong P.W., "Inverse halftoning and kernel estimation for error diffusion", *IEEE Trans. on Image Processing*, vol. 4, no. 4, pp. 486-498, 1995.

[32] Wong P.W. and N.D. Memon, "Image Processing for Halftones", *IEEE Signal Processing Magazine*, vol. 20, no. 4, July 2003.